Oxid Met (2011) 76:1–21
DOI 10.1007/s11085-011-9254-6

REVIEW

Hot Corrosion of Metals and Alloys

Fred Pettit

Received: 17 January 2011 / Revised: 26 April 2011 / Published online: 20 May 2011

Abstract When metals and alloys are used at high temperatures, especially in combustion processes, deposits often accumulate on the metal surfaces and affect the oxidation processes. This paper is concerned with deposit-induced accelerated corrosion, or hot corrosion, of metals and alloys. Initially, the characteristics of hot corrosion are identified for Na_2SO_4 deposits in terms of the factors that influence the reaction process. It is shown that hot corrosion consists of initiation or incubation and propagation stages. During the initiation or incubation stage, the deposit is shown to not have a significant effect on the corrosion processes, but it is causing conditions to develop whereby the propagation stage characteristics are determined with attendant large increases in the corrosion rates. Type I, high temperature hot corrosion and Type II, low temperature hot corrosion are then described in terms of historical mechanistic perspectives. The dependence of Type I and Type II hot corrosion on temperature and SO_3 partial pressure is discussed along with future work that is needed in order to more completely understand these hot corrosion processes along with the effects of some elements such as Cr, Al, Mo, Co and Pt.

Keywords Hot corrosion · Mechanisms · Transitions · Type I · Type II

Introduction

When metals and alloys are used at elevated temperatures, especially in equipment that involves combustion, deposits, usually liquid, can accumulate on component hardware whereby the deposits can have a profound influence on the corrosion process involved in the degradation of the alloys. This process of deposit-induced accelerated oxidation is called hot corrosion. The origin of the name comes from the

F. Pettit (✉)
University of Pittsburgh, 848 Benedum Hall, 3700 O'Hara St., Pittsburgh, PA 15261, USA
e-mail: pettitfs@pitt.edu

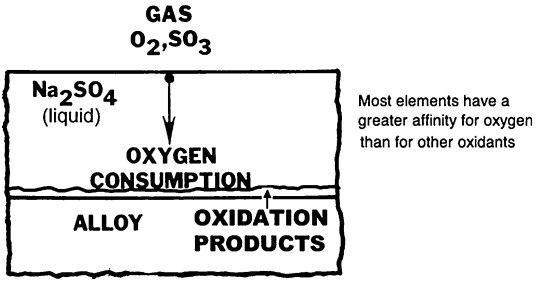

Fig. 1 Schematic drawing illustrating conditions that cause hot corrosion of metals and alloys

similarity of these conditions to aqueous corrosion in which a liquid, aqueous medium plays a significant role in the degradation process.

The degradation of alloys due to hot corrosion has been a serious problem for at least 80 years, and there are numerous papers and reviews [e.g., 1–4] on this process. There are a number of different deposits that have been shown to cause hot corrosion of alloys. Such deposits include sulfates of Na, Ca, and K, as well as vanadates and carbonates. In fact, as illustrated in Fig. 1, deposits on the surfaces of alloys separate the alloys from the gas environments and providing that transport through the deposit is slow, some reaction between elements in the alloy and components in the deposit are likely. Therefore, most deposits can exert some influence on the oxidation characteristics of alloys.

In gas turbines a common deposit is Na_2SO_4 where the sodium and sulfur may exist as impurities in the fuel, or NaCl as well as sulfates may be ingested in the air required for combustion and the NaCl is converted to Na_2SO_4 via reaction with sulfur in the fuel. In this paper the effects of Na_2SO_4 deposits will be considered, however, what is discussed is relevant to other deposits that are liquid or can react to form a liquid under the exposure conditions.

The objectives of this paper are to provide a consistent description of the hot-corrosion process emphasizing the important mechanisms and their dependence on temperature and SO_3 partial pressure in the gas. Initially the important characteristics of the hot corrosion process will be identified and then the mechanisms by which hot corrosion occurs will be discussed. It will be shown that the characteristics of hot corrosion, as well as the effects of different elements, depend upon the particular mechanism by which the hot corrosion is occurring.

The Characteristics of Hot Corrosion

The characteristics of hot corrosion attack are numerous. The Na_2SO_4 deposit causes a non-protective scale to form on the alloy or metal, whereas a protective scale is formed by reaction with the gas in the absence of the deposit. It is important to emphasize that the attack may not be self-sustaining in that a protective scale eventually forms unless additional deposit arrives upon the surface of the alloy, Fig. 2.

The hot corrosion attack is influenced by the exposure time, as shown in Fig. 3, where the attack consists of an initiation or incubation stage and a propagation

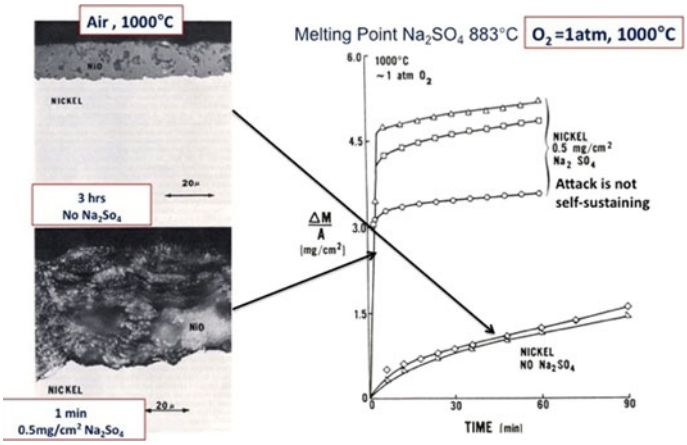

Fig. 2 In Fig. 2 the weight change versus time data for nickel with and without a Na_2SO_4 deposit are compared. The Na_2SO_4 deposit causes an initial large weight gain followed by much smaller subsequent weight gains and, during the period of large weight gains, a nonprotective NiO scale develops on the nickel specimen

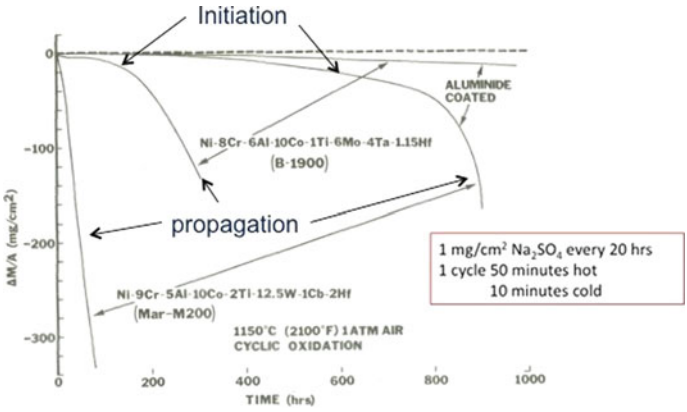

Fig. 3 In Fig. 3 data are presented for uncoated superalloys and for aluminide coated superalloys. Both types of specimens undergo hot corrosion attack but the aluminide coated specimens require many cycles at temperature before the propagation stages are reached

stage. In the initiation stage the alloy is behaving much as it would by reacting with the gas in the absence of the deposit whereas, in the propagation stage, the deposit exerts a profound effect on the attack.

Most cases of deposit-induced accelerated attack occur when the deposit is a liquid; although, some examples of attack caused by solid deposits are available [5], but no attack has been reported when the substance comprising the deposit exists as a gas [6]. Such effects of the physical state of the deposit are related to conditions that can develop as the alloy reacts with the deposit in the absence of effects caused by reaction with the gas. As shown in Fig. 4, a liquid Na_2SO_4 deposit can result in

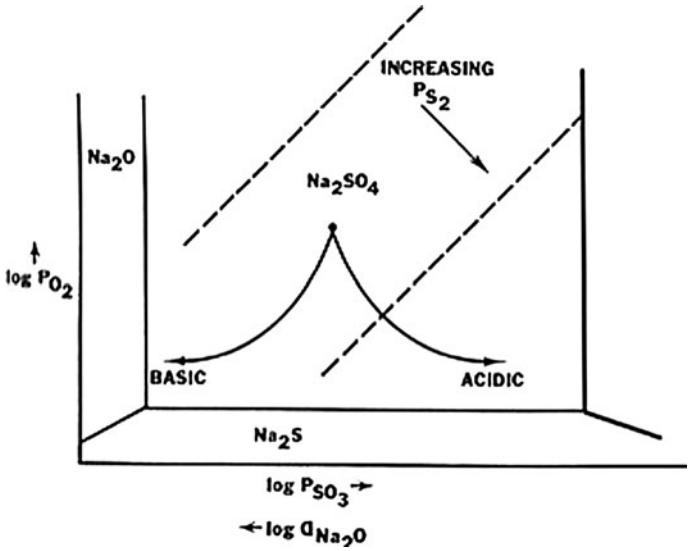

Fig. 4 A thermodynamic stability diagram for sodium, sulfur and oxygen that shows how Na_2SO_4 can change in composition due to reaction. The basic conditions arise via the removal of oxygen and sulfur from the Na_2SO_4 by the alloy. The acidic conditions can arise due to the formation of refractory metal oxides resulting from the oxidation of refractory metals in the alloy. The basic and acidic characteristics of Na_2SO_4 are related by applying the law of mass action to Eq. 1. The *dashed lines* indicate sulfur isobars

the Na_2SO_4 developing basic (excess Na_2O) or acidic (excess SO_3) characteristics. By applying the law of mass action to Eq. 1,

$$Na_2O + SO_3 = Na_2SO_4 \quad (1)$$

the acidic and basic characteristics of the Na_2SO_4 can be related to one another. Such effects can have substantial influence on the hot-corrosion process, as will be discussed subsequently. The hot corrosion of alloys is dependent upon the amount of the deposit as shown in Fig. 5 where the weight gain of a Ni–8Cr–6Al[1] specimen is substantially greater as the amount of Na_2SO_4 is increased. However, exceptions do exist, for example, when the effects of the Na_2SO_4 are induced by an element in the alloy, in this case Mo in the Ni–8Cr–6Al–3Mo, since a thin layer of Na_2SO_4 causes attack after a shorter exposure time than a thicker layer, Fig. 5.

The composition of the deposit plays a significant role in the hot corrosion process. This is shown in Fig. 6 where Ni–30Cr and Ni–25Cr–6Al specimens are exposed to Na_2SO_4–NaCl deposits at 900 °C in air. In the absence of such deposits an alumina layer is formed on the Ni–25Cr–6Al specimen whereas a Cr_2O_3 scale is formed on the Ni–30Cr specimen. The attack of both alloys increases as the amount of NaCl in the deposit is increased but the attack of the Ni–30Cr alloy is more severe compared to that of the Ni–25Cr–6Al alloy.

[1] All compositions are in weight percent unless stated otherwise.

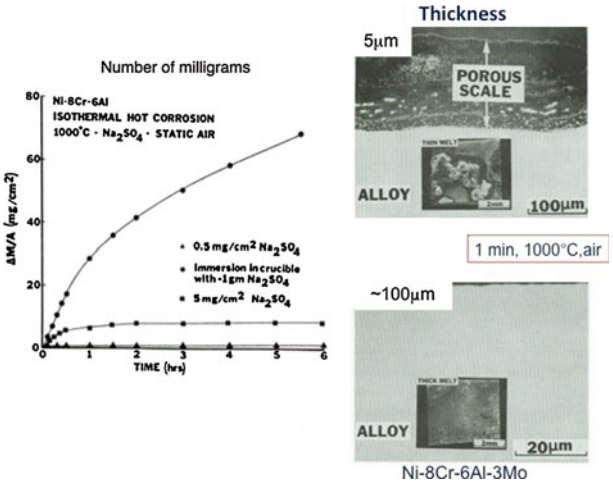

Fig. 5 Data to show how the hot corrosion attack of alloys can be affected by the amount of the deposit. In the case of the Ni–8Cr–6Al–3Mo alloy the thicknesses of the Na_2SO_4 deposits were 5 and 100 micrometer

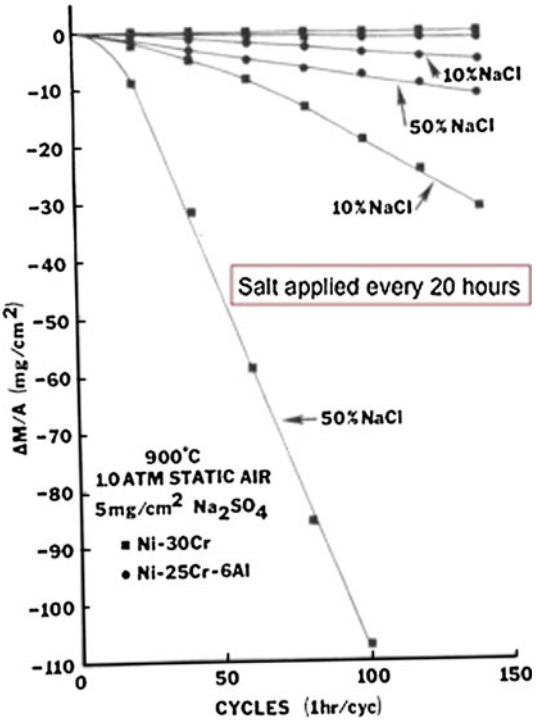

Fig. 6 Weight change versus time measurements for the cyclic oxidation of two alloys with Na_2SO_4–NaCl deposits which show that the composition of the deposits affects the hot corrosion of the alloys

The hot corrosion process is influenced by the temperature. This is shown schematically in Fig. 7. As the temperature is increased the attack changes from what is called low temperature attack, Type II, to high temperature attack, Type I.

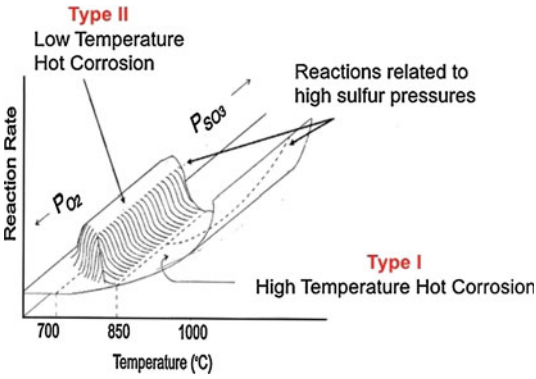

Fig. 7 Schematic to illustrate the different hot corrosion attack regimes as a function of temperature and SO_3 partial pressure. Reaction rate surfaces are presented to show the various hot corrosion processes

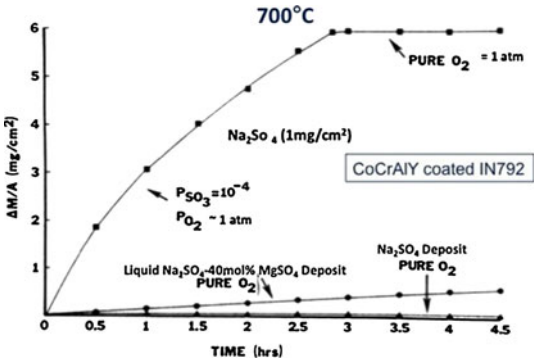

Fig. 8 Weight change versus time measurements to show how the Na_2SO_4 induced attack of a CoCrAlY coating is influenced by the SO_3 partial pressure in the gas phase. Na_2SO_4 is solid at 700 °C and a Na_2SO_4–$MgSO_4$ mixture was used to produce a liquid at 700 °C

These two types of hot corrosion are also affected by the gas composition which will be discussed subsequently. Type I hot corrosion was first encountered in aircraft gas turbines. Type I degradation microstructures could be reproduced in laboratory experiments at 900–950 °C using Na_2SO_4 deposits and exposure in air or oxygen. As gas turbines began to be used for marine propulsion, another type of hot corrosion was observed and it was determined that in order to reproduce the Type II microstructure, it was necessary to have SO_3 present in the gas [7]. As a result of the observation that SO_3 should be present to cause hot corrosion attack a number of experiments were performed over the temperature range from 650 °C to 950 °C using oxygen–SO_2 gas mixtures. At temperatures from 650 °C to 750 °C, low temperature, Type II, attack was only observed when SO_3 gas pressures were established in the gas mixture, Fig. 8. However, high temperature, Type I, hot corrosion could occur at temperatures of 900 °C to 950 °C in gas mixtures of air or pure oxygen, Fig. 9. When low temperature hot corrosion was first observed and efforts were made to describe why it occurred, NaCl deposits on alloys were considered as possible causes. As can be seen in Fig. 6, NaCl does cause attack of alloys but the microstructure of degraded specimens is not the same as that for low temperature hot corrosion. The NaCl reacts with chromium and aluminum in alloys to form gaseous chlorides that result in porous chromia and alumina scales upon reaction with oxygen.

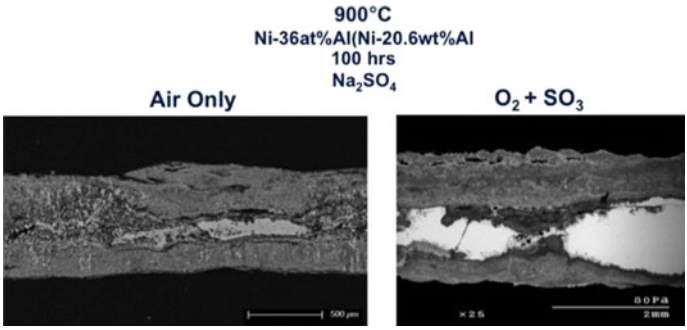

Fig. 9 Comparison of the degradation occurring for the Na_2SO_4 induced attack of an alloy in air and in oxygen with SO_3. Severe attack occurred in air as well as in a gas with SO_3

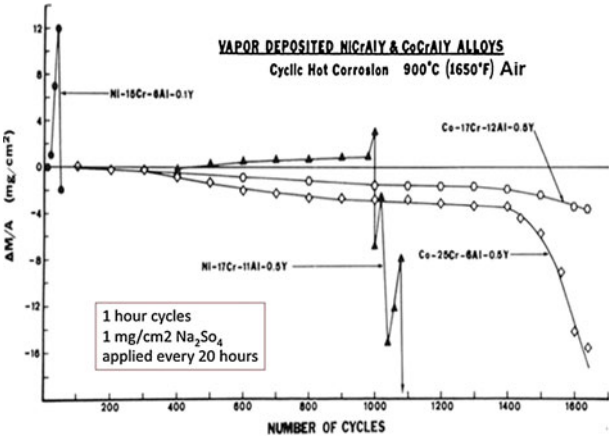

Fig. 10 Weight change versus time measurements for the cyclic oxidation of a number of alloys with Na_2SO_4 deposits are presented. The onset of severe attack as indicated by large weight gains or losses is dependent upon alloy composition

The hot corrosion of alloys is dependent upon alloy composition as shown in Fig. 10. The test conditions to initiate the hot corrosion of the alloys in Fig. 10 consisted of Na_2SO_4 applied every 20 h. The test is at 900 °C in air where the specimens were cycled from the test temperature to room temperature every hour. It can be seen that the CoCrAlY specimens are much more resistant to hot corrosion under these Type I conditions compared to the NiCrAlY specimens. It should also be noted that depending upon the alloy composition relatively long test times can be required to initiate the propagation mode of hot corrosion attack.

The hot corrosion process is also dependent upon other factors such as the fabrication condition of the alloys which influences their microstructures, the gas velocity in the test, cyclic versus isothermal conditions, erosive particles and specimen geometry. These factors will not be discussed in this paper. All of these factors are relevant because they affect the protectiveness of the oxide scales that

form on alloys during the initiation stage of hot corrosion, or the availability of certain elements in the alloy to the Na_2SO_4 deposit.

Some of what has been presented in the previous paragraphs may seem to be inconsistent. This occurs because Type I and Type II hot corrosion occur via different, but related, mechanisms. In order to develop consistency it is necessary to consider the mechanisms by which these two types of hot corrosion take place.

High Temperature, Type I, Hot Corrosion

Hot corrosion attack was first observed in boilers and gas turbines in the period between 1930 and 1960 [8]. In the case of boilers the temperatures were about 540 °C with liquid deposits of $Na_3Fe(SO_4)_3$. In the 1960s Type I attack was observed in aircraft gas turbines at temperatures of 900 °C with Na_2SO_4 deposits. As shown in Fig. 11, this attack appeared to be related to the oxidation of sulfides in the alloys where the sulfur came from the Na_2SO_4 deposits and consequently this type of hot corrosion was frequently called "sulfidation" [9]. Bornstein and DeCrescente [6, 10] performed experiments using the alloy B-1900 and showed that when the amount of sulfur in 1 mg/cm^2 of Na_2SO_4 was introduced into this alloy no hot corrosion attack occurred upon subsequent oxidation, but substantial attack of this alloy took place with deposits (1 mg/cm^2)of Na_2SO_4 or Na_2NO_3. They concluded that the hot corrosion attack of this alloy occurred because of the Na_2O component in the Na_2SO_4 or Na_2NO_3. It was proposed that the Na_2O destroyed the normally protective oxide scale that usually developed on this alloy due to a basic fluxing reaction as indicated in the following for a NiO scale

$$NiO + Na_2SO_4 = 2Na^+ + NiO_2^{2-} + SO_3 \quad (2)$$

Rapp and Goto [11] examined the hot corrosion fluxing process and proposed that a negative solubility gradient was necessary whereby the oxide on the alloy dissolved in the molten deposit at the scale/deposit interface, but precipitated out in the deposit where the solubility was lower as a discontinuous scale, as illustrated in Fig. 12a. Rapp and his students determined the solubility of a number of oxides in

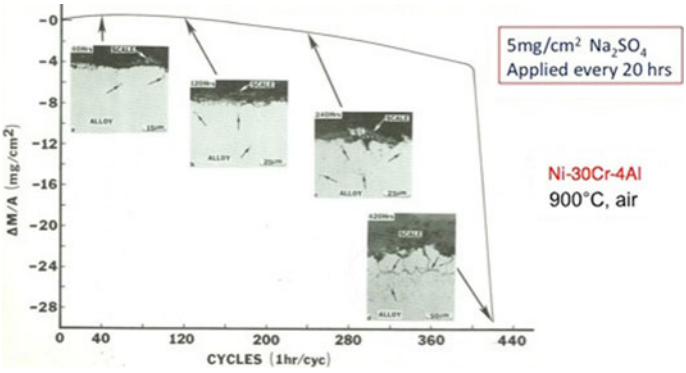

Fig. 11 Weight change versus time measurements for Na_2SO_4 deposits on a Ni–30Cr–4Al alloy and the resulting degradation microstructures showing sulfide formation and oxidation

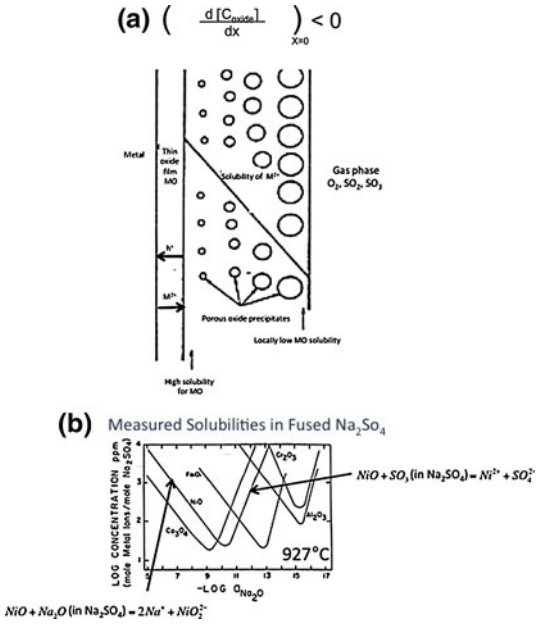

Fig. 12 **a** Sketch describing the negative solubility gradient where an oxide dissolves and reprecipitates out in the Na_2SO_4. **b** Solubilities of oxides in fused Na_2SO_4 with reactions describing the dissolution process

Na_2SO_4 as a function of the activity of Na_2O in the Na_2SO_4 and showed that the solubilities could be rationalized via reactions with the Na_2O or SO_3 components in the Na_2SO_4, Fig. 12b [12].

In considering how the Na_2O activity in a Na_2SO_4 deposit on nickel could increase to levels whereby NiO dissolved into the Na_2SO_4, Goebel and Pettit [13] observed that at 900 °C Na_2SO_4 did not decompose rapidly in air or oxygen via the reaction

$$Na_2SO_4 = Na_2O + SO_3 \tag{3}$$

It was proposed that the liquid Na_2SO_4 layer separated the nickel specimen from the oxygen gas, and consequently an oxygen gradient was established across the Na_2SO_4 from the gas interface to the nickel interface. As a result of this gradient in the Na_2SO_4, as shown in Fig. 13, the sulfur activity was increased to levels such that sulfur could penetrate the oxide scale formed on the nickel to form nickel sulfide in the nickel. The removal of oxygen and sulfur from the Na_2SO_4 caused the activity of Na_2O in the Na_2SO_4 to increase as shown in the following reaction,

$$\begin{aligned} Na_2SO_4 = {} & Na_2O(\text{in } Na_2SO_4) + \frac{3}{2}O_2(\text{used to form NiO}) \\ & + \frac{1}{2}S_2(\text{used to form Ni sulfide}) \end{aligned} \tag{4}$$

The activity of Na_2O was greatest at the NiO/Na_2SO_4 interface and decreased in the Na_2SO_4 layer towards the Na_2SO_4/gas interface. The Rapp-Goto solubility criterion was satisfied and NiO dissolved at the NiO/Na_2SO_4 interface and precipitated as discontinuous particles in the outer regions of the Na_2SO_4. The reaction that occurred at the oxide/salt interface was

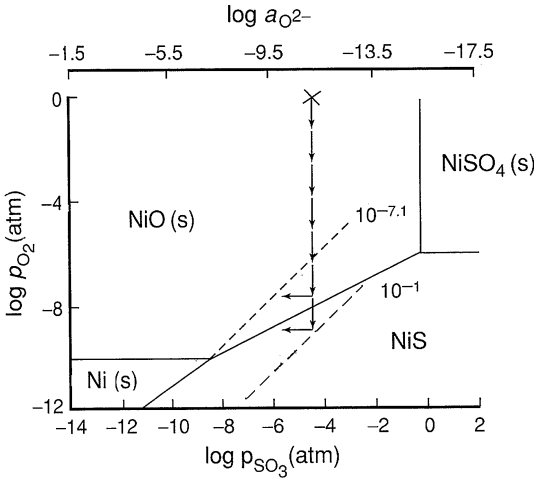

Fig. 13 Stability diagram showing the phases of nickel that are stable in the Na_2SO_4 region of Fig. 4 at 1000 °C. The *dashed lines* are sulfur isobars and the *arrows* indicate how the composition of the Na_2SO_4 can change due to oxygen and sulfur removal from the initial composition. X indicates the as deposited composition of the Na_2SO_4

$$NiO + Na_2O(\text{in } Na_2SO_4) = Na_2NiO_2 \quad (5)$$

with the reverse of this reaction occurring out in the Na_2SO_4 deposit. The reaction by which the NiO precipitates provides Na_2O to the Na_2SO_4 and eventually the negative solubility gradient is removed and the fluxing reaction stops. In particular, this type of hot corrosion is not self sustaining.

Much of the experimental work to study Type I attack was performed in air or pure oxygen, but with the advent of studies on Type II attack the importance of SO_3 in the gas became apparent. A question that became relevant was," how important is SO_3 in the gas for the case of Type I attack"? In order to answer this question, Rapp and Otuska [14] performed experiments with preoxidized nickel with a Na_2SO_4 deposit in an oxygen–SO_2 gas mixture and measured the Na_2O activity and oxygen pressure at the NiO/Na_2SO_4 interface as a function of time. The results are presented in Fig. 14 where a stability diagram is used to show the phases of nickel that are stable as a function of the Na_2O activity and oxygen partial pressure. The times at which these measurements were made are also indicated on this stability diagram. It can be seen that as the oxygen pressure is decreased substantially due to reaction with nickel and the region of sulfide stability is entered, the activity of Na_2O increases due to oxygen and sulfur removal from the Na_2SO_4. The point to be emphasized is that the effects due to reaction of the Na_2SO_4 with the nickel override any influence of the gas environment. Consequently the attack is not dependent on the composition of the gas in the case of nickel.

In considering the Type I mechanism it appears that both basic fluxing and sulfide formation followed by oxidation of these sulfides take place concomitantly. In Fig. 15 cyclic oxidation data are presented for a Ni–25Cr–6Al alloy where this alloy was coated with Na_2SO_4 every 5 h up to 20 h and then after every 10 h. Other specimens were sulfidized in an H_2S/H_2 gas mixture at the same time intervals where the amount of sulfur added to the specimens was the same as that in the Na_2SO_4 deposits. Inspection of Fig. 15a shows that the degradation of both specimens is similar showing, in contrast to the results of Bornstein and

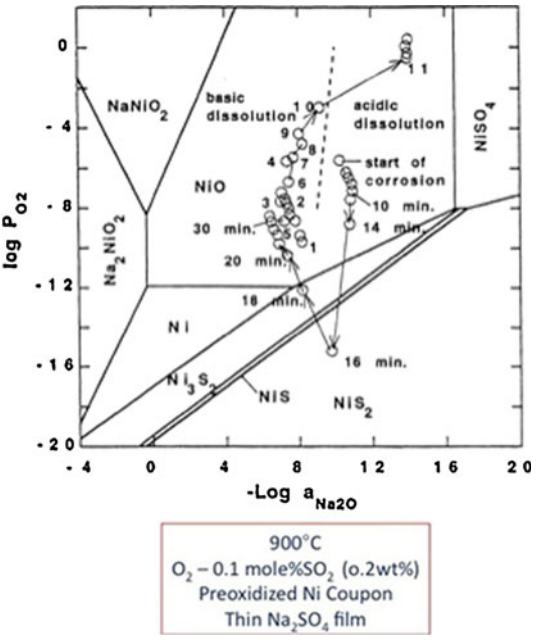

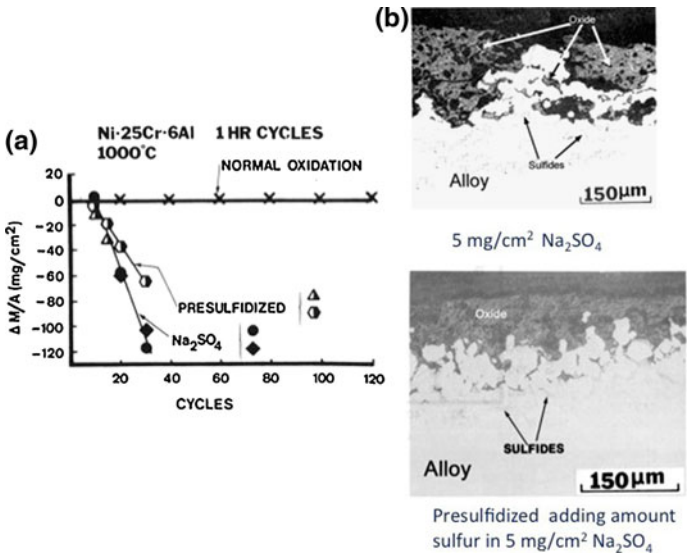

Fig. 14 Sketches using a nickel–oxygen–sulfur thermodynamic stability diagram to show the oxygen and Na_2O activity values at the NiO/Na_2SO_4 interface as a function of time. The *dashed line* indicates the change in the dissolution process from basic to acidic. Exposure times are in minutes and hours (not labeled)

Fig. 15 Weight change versus time measurements for Ni–25Cr–6Al oxidized in air with Na_2SO_4 deposits and presulfidized specimens where the sulfur added to the specimen was the same as that in the Na_2SO_4 deposits (**a**). Micrographs of the specimens after conclusion of the test (**b**)

DeCrescente, that the sulfur in the Na_2SO_4 can cause substantial attack of alloys in cyclic oxidation. As shown in Fig. 15b, the microstructures of the exposed specimens are similar. These results are not consistent with the results of Bornstein

and DeCrescente because those investigators used the alloy B-1900 in their studies. As will be shown this alloy undergoes catastrophic hot corrosion due to the Mo in the alloy reacting with Na_2SO_4, or $NaNO_3$, to form Na_2MoO_4 with a high activity of MoO_3. Protective scales such as alumina undergo alloy-induced acidic fluxing involving the following reaction

$$Al_2O_3 + 3MoO_3(\text{in } Na_2MoO_4) = 2Al^{3+} + 3MoO_4^{2-} \quad (6)$$

There is a negative solubility gradient in the Na_2MoO_4 because MoO_3 is removed from the liquid solution at the gas interface due to vaporization. This process can occur with Na_2SO_4 or $NaNO_3$ deposits but not when the sulfur from the $Na2SO_4$ is added to this alloy via an H_2S–H_2 gas mixture.

Some investigators have studied the attack of alloys with Na_2SO_4 deposits in O_2–SO_2 gas mixtures where the SO_2 concentrations were high ($\sim$4%) which established SO_3 gas pressures on the order of 10^{-2} atm [15–17]. Table 1 presents the SO_3 partial pressures in different O_2–SO_2 gas mixtures as well as the SO_3 pressures to form Na_2SO_4 and $CoSO_4$ at different temperatures. The results of such studies show that at both 700 °C and 900 °C a substantial number of sulfides is formed in alloys and the degradation consists of oxidation of these sulfides. It therefore appears that there are regimes involving degradation of alloys at temperatures and SO_3 pressures where the hot corrosion process consists predominantly of this sulfidation mode as shown in Fig. 7.

In some cases of hot corrosion, one application of Na_2SO_4 can result in catastrophic attack of the alloys whereby the alloy is completely converted to corrosion products. In such cases the hot corrosion process involves the oxides of certain elements in the alloy, usually refractory metals such as Mo or W whereby the Na_2SO_4 is converted to a molybdate or tungstate and SO_3 is evolved as shown in the following reaction,

$$Na_2SO_4 + MoO_3 = Na_2MoO_4 + SO_3(\text{gas}) \quad (7)$$

In such cases the molten deposit can be considered to have two acidic components, namely SO_3 and MoO_3, and the solubility of the protective oxide is different depending upon the acidic oxide as shown in Fig. 16. Moreover the Rapp-Goto solubility criterion is satisfied because the acidic component formed by oxidation of an element in the alloy is usually volatile. This form of hot corrosion, which has been called alloy-induced acidic fluxing, is observed at temperatures between 900 °C and 1000 °C. A comparison of this type attack to basic fluxing-

Table 1 Some Data Concerning Sulfate Formation and SO_3 Pressures

Temperature	P_{SO_2} Liquid fuel 0.5 wt% S	P_{SO_2} to form Na_2SO_4	P_{SO_2} to form $CoSO_4$	P_{SO_2} O_2–0.1 wt% SO_2	P_{SO_2} O_2–1 wt% SO_2	P_{SO_2} O_2–3 wt% SO_2
1200 K (927 °C)	2.7×10^{-4}	1.8×10^{-17}	3.1×10^{-2}	1.0×10^{-4}	1.3×10^{-3}	3.8×10^{-3}
1100 K (827 °C)	3.7×10^{-4}	1.6×10^{-19}	3.6×10^{-3}	3.0×10^{-4}	3.1×10^{-3}	9.1×10^{-3}
1000 K (727 °C)	4.4×10^{-4}	5.1×10^{-22}	3.0×10^{-4}	9.0×10^{-4}	9.0×10^{-3}	2.7×10^{-2}
900 K (627 °C)	4.8×10^{-4}	4.5×10^{-25}	1.0×10^{-3}	3.3×10^{-3}	3.3×10^{-2}	9.8×10^{-2}

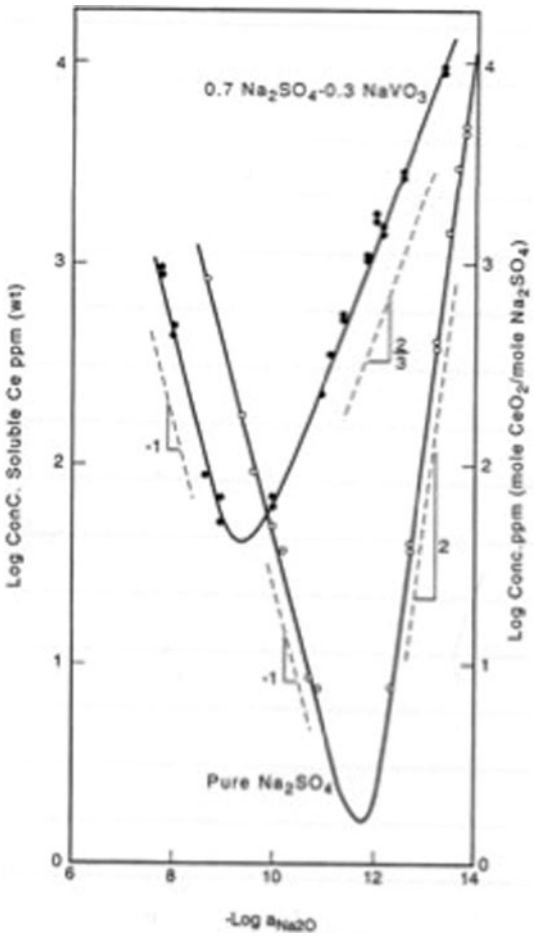

Fig. 16 Solubility curves for CeO_2 in Na_2SO_4 and in Na_2SO_4–30%$NaVO_3$ at 900 °C. The slopes of the solubility curves are similar in the basic region, but different in the acidic region because the basic component is the same in both melts but there are two acidic components, namely SO_3 and V_2O_5

sulfidation is shown in Fig. 17 where weight change versus time measurements are presented for Na_2SO_4 deposits on Ni–25Cr–6Al and Ni–25Cr–6Al–6Mo. Both alloys show increased attack via basic fluxing-sulfidation but the alloy with Mo has a catastrophic amount of attack due to the conversion of the Na_2SO_4 to Na_2MoO_4 and the alloy-induced attack. Mishra [15] has shown that the alloy-induced acidic fluxing process is influenced by the SO_3 pressure in the gas phase, Fig. 18. Rapid attack of the alloy U-700 was observed with small concentrations of SO_2 in the gas but the attack was found to decrease as the SO_2 concentration approached 1 and 2%. This can be explained by applying the law of mass action to Eq. 7 and assuming the Na_2SO_4–Na_2MoO_4 solution is ideal. One obtains

$$a_{MoO_3} = (1 - N_{Na_2SO_4})p_{SO_3}/N_{Na_2SO_4}K \quad (8)$$

It can be seen that the a_{MoO_3} in the Na_2SO_4–Na_2MoO_4 solution is dependent upon the mole fraction of Na_2SO_4 in the solution and the SO_3 pressure. When the SO_3

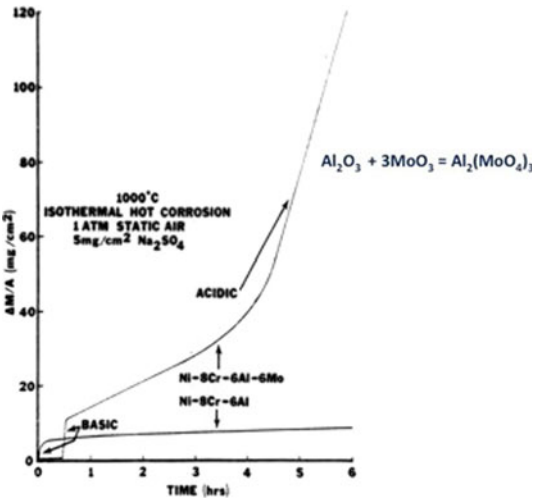

Fig. 17 Weight change versus time measurements for the Na_2SO_4-induced hot corrosion attack of two alloys with similar compositions but with one alloy containing Mo. Both alloys are degraded initially via basic fluxing but the alloy containing Mo eventually undergoes alloy-induced acidic fluxing

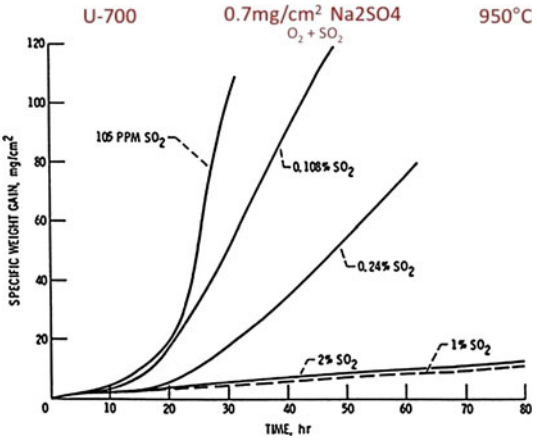

Fig. 18 The alloy U-700 is shown to exhibit alloy induced acidic fluxing, but this type of attack is inhibited as the SO_3 pressure is increased since this attack is influenced by the mole fraction of Na_2SO_4 in the sulfate solution

pressure is low the Na_2SO_4 is converted to Na_2MoO_4 and $N_{Na_2SO_4}$ approaches zero whereby the activity of MoO_3 is high. However, for high values of SO_2 the mole fraction of Na_2SO_4 in the Na_2SO4–Na_2MoO_4 solution is significant and consequently the activity of MoO_3 is low. Hence alloy-induced acidic fluxing does not occur. In this latter case, Mishra [15] has shown the attack occurs via a sulfide formation and oxidation of sulfide mode.

Type I hot corrosion attack has been shown to be induced via liquid Na_2SO_4 deposits whereby oxygen and sulfur removal from the Na_2SO_4 causes the Na_2O activity in the Na_2SO_4 to be increased to levels at which oxides such as NiO and Al_2O_3 can be fluxed from the alloy surface and precipitated out in the Na_2SO_4 as discontinuous particles. This process has been shown to be unaffected by the composition of the gas phase but more work is required especially with alloys resistant to this type of attack, to further examine gas effects on Type I hot corrosion.

Low Temperature Type II Hot Corrosion

The observation of Type II hot corrosion was made in the 1970s in gas turbines used for marine propulsion. The degradation microstructure was much different than those caused by basic fluxing-sulfidation and alloy-induced acidic fluxing as can be seen in Fig. 19. The Type II microstructure often consisted of pits that extended into the alloy, Fig. 20. At the corrosion product-gas interface the pit was enriched in cobalt or nickel depending upon the base element of the alloy. However, the concentrations of these two elements decreased as the pit was entered going toward the alloy. The aluminum and chromium concentrations in the pit had the distributions similar to those in the alloy which suggested that these two elements were converted to oxides in situ with little or no diffusion. In the case of CoCrAlY coatings, which were very susceptible to this type of attack, no sulfides were evident in the alloy adjacent to the corrosion product, Fig. 20. However, as the nickel content of the alloy was increased sulfides at such locations were evident, Fig. 21. Furthermore, in the case of CoCrAlY alloys sulfur was detected in the corrosion product adjacent to the alloy, Figs. 20 and 21, but no sulfur containing compounds were detected.

A number of mechanisms have been proposed to account for the Type II degradation process [18–20]. All of these mechanisms propose that at temperatures of 650 °C to 750 °C solid Na_2SO_4 is converted to a liquid solution of Na_2SO_4–$CoSO_4$ or Na_2SO_4–$NiSO_4$, Fig. 22, via the conversion of CoO or NiO to sulfates due to reaction with SO_3 in the gas. In the case of CoCrAlY alloys, the mechanism proposed by Luthra [18] is probably the most accurate. In this mechanism a liquid Na_2SO_4–$CoSO_4$ solution develops upon the alloy surface. The compositional limits of this sulfate solution are shown in Fig. 23 where the cobalt–oxygen–sulfur phase stability diagram is used to describe its limits. It can be seen that this sulfate solution has a composition where CoO, Co_3O4 and $CoSO_4$ can be stable. In the CoO region the SO_3 minimum pressure is obtained by determining the activity of $CoSO_4$

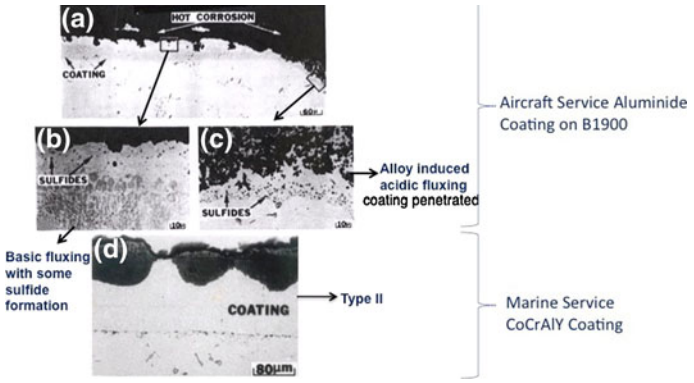

Fig. 19 Micrographs comparing the microstructures of alloys that have undergone Type I and Type II hot corrosion attack as well as alloy-induced acidic fluxing

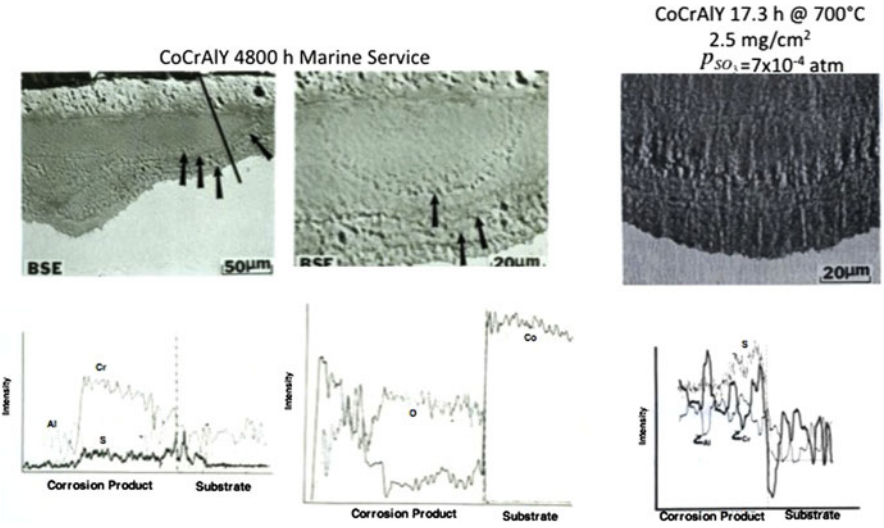

Fig. 20 Microstructures and concentration profiles for a CoCrAlY alloy degraded via Type II hot corrosion in a laboratory test and after marine service. The *arrows* indicate the location of the corrosion front after shorter exposure times

necessary to form a liquid phase. This activity is 0.03 at 750 °C [18] and the SO_3 pressure is calculated from the following reaction,

$$CoO + SO_3 = CoSO_4 \tag{9}$$

This SO_3 pressure exists over a range of oxygen pressures up to the CoO/Co_3O_4 equilibrium. Above this oxygen pressure the following reaction must be used to calculate the SO_3 pressure,

$$\tfrac{1}{3}Co_3O_4 + SO_3 = CoSO_4 + \tfrac{1}{6}O_2 \tag{10}$$

It can be seen, Fig. 23, that the SO_3 pressure increases with the oxygen pressure. The total pressure in the gas phase cannot exceed 1 atm since laboratory experiments at 1 atm total pressure caused Type II hot corrosion attack. This limits the oxygen pressure that can be in equilibrium with Co_3O_4 to approximately 1 atm. At this oxygen limit the SO_3 pressure will be determined by the amount of sulfur in the gas and can be sufficient to form $CoSO_4$ at unit activity. In the case of these higher SO_3 pressures the oxygen pressure can vary from 1 atm down to values at which the SO_2 pressure approaches 1 atm where the SO_2 pressure can be calculated from the reaction,

$$SO_3 = SO_2 + \tfrac{1}{2}O_2 \tag{11}$$

Luthra proposes that SO_3 is transported from the gas through the Na_2SO_4–$CoSO_4$ liquid via $S_2O_7^{2-}$ ions involving an exchange reaction with SO_4^{2-}. The reaction at the salt/gas interface consists of

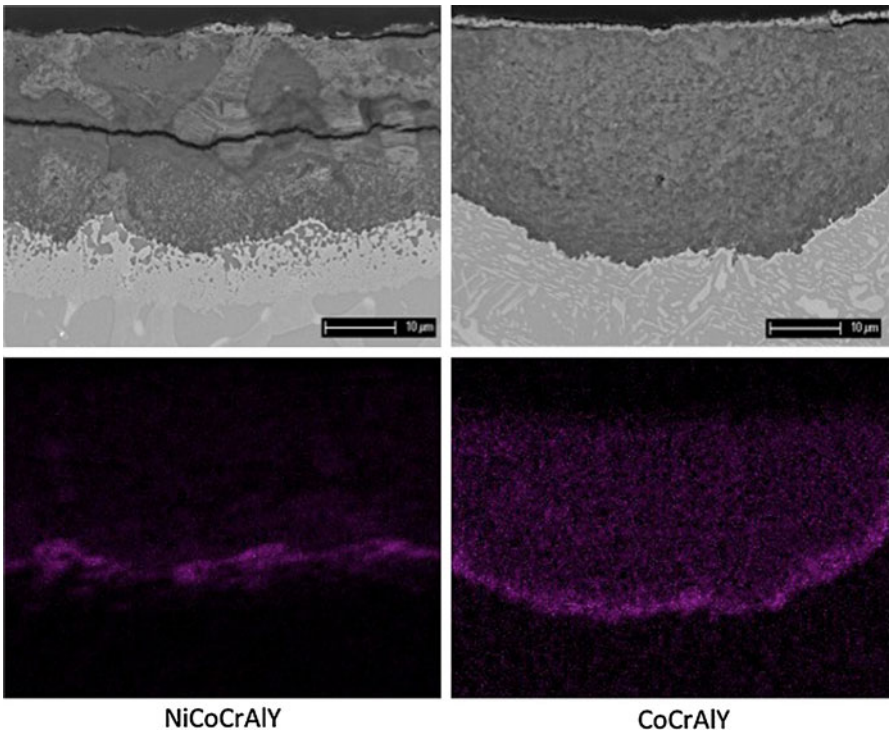

Fig. 21 Scanning electron micrographs and X-ray maps for sulfur for NiCoCrAlY and CoCrAlY specimens exposed for 10 h at 700 °C whereby hot corrosion attack occurred

$$SO_4^{2-} + SO_3 = S_2O_7^{2-} \tag{12}$$

The following reaction provides oxygen and sulfur at the scale/sulfate interface

$$S_2O_7^{2-} = SO_4^{2-} + SO_2 + \frac{1}{2}O_2 \tag{13}$$

It is also proposed that Co ions are diffusing in the liquid sulfate, namely, Co^{2+} outward and Co^{3+} inward. The important species and reactions are presented in Fig. 24. Cobalt goes into the liquid sulfate at the scale/sulfate interface as Co^{2+} and $Co3O_4$ is precipitated out in the liquid sulfate near the gas interface. (If the SO_3 pressure is sufficiently high, $CoSO_4$ can be precipitated rather than Co_3O_4.) Oxygen and sulfur are supplied to the alloy whereby oxides and sulfides of cobalt, chromium and aluminum are formed. The dissolution of cobalt from the alloy causes any Cr_2O_3 or Al_2O_3 that are formed to be discontinuous and no protective oxide barrier can be developed.

The Type II mechanism that has been presented is applicable to some alloys but perhaps not to all alloys. Moreover at high SO_3 pressures it has been observed that extensive sulfide formation is part of the attack [15–17]. As shown in Fig. 25, there is a need to examine the transition from Type II attack to sulfide formation and oxidation at 700 °C and from Type I attack to sulfide formation at 900 °C.

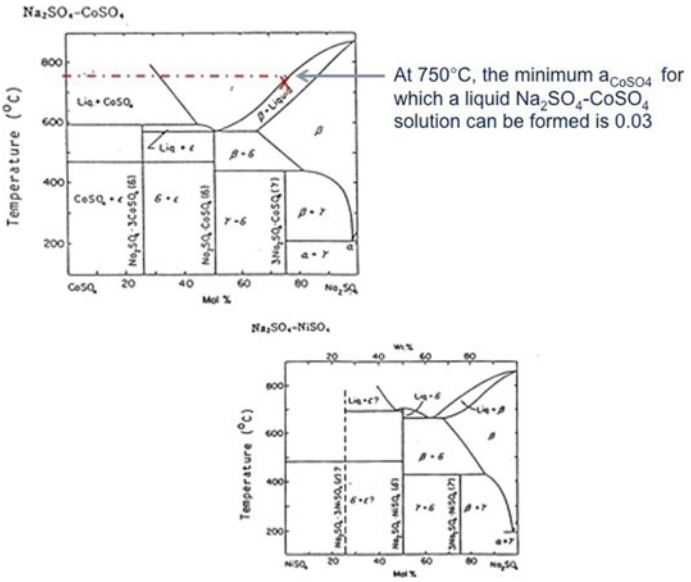

Fig. 22 Phase diagrams for $CoSO_4$–Na_2SO_4 and $NiSO_4$–Na_2SO_4 showing the compositions of low melting eutectics. The lowest activity of $CoSO_4$ in Na_2SO_4 to form a liquid at 750 °C is 0.03

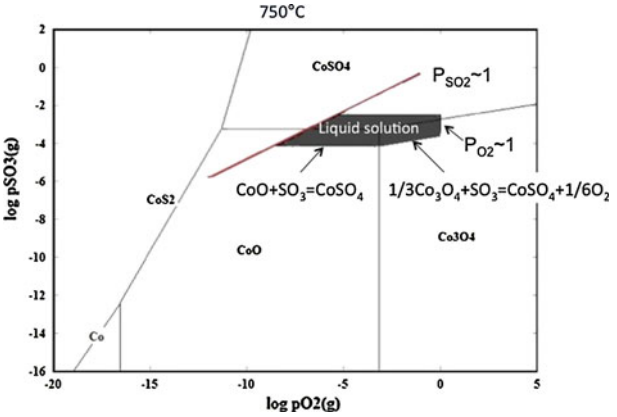

Fig. 23 Diagram showing the region where a liquid $CoSO_4$–Na_2SO_4 solution can exist when a Na_2SO_4 deposit is present on a CoCrAlY alloy at 750 °C in a gas mixture of oxygen–2% SO_2

Concluding Remarks

This paper has attempted to use the results that are available in the literature to explain the phenomena of Type I and Type II hot corrosion and to identify research that is necessary to further clarify the interrelationships between these two deposit-induced degradation processes as well as the effects produced by some of the

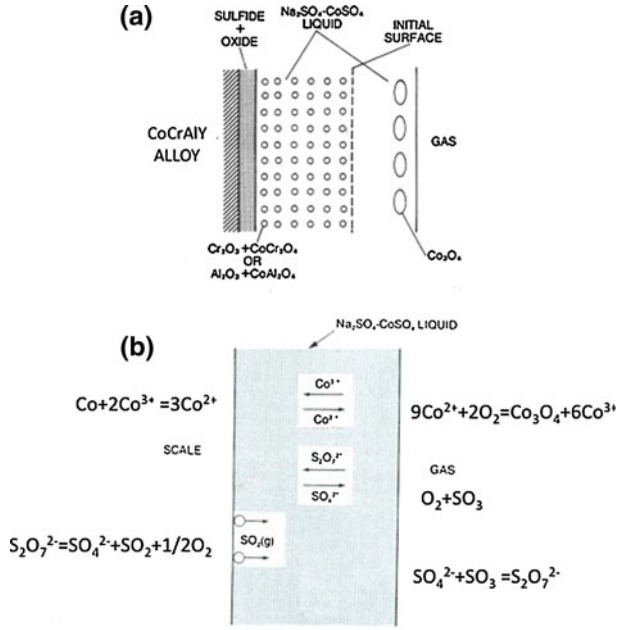

Fig. 24 Sketches to show features of Type II attack of CoCrAlY (**a**), along with the important diffusing species and reactions (**b**)

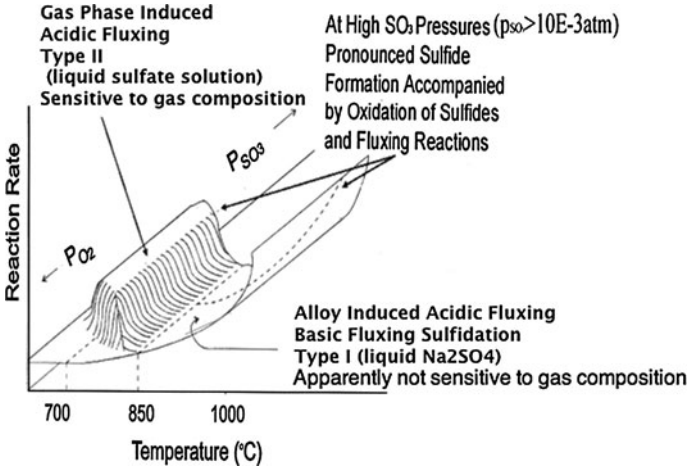

Fig. 25 Summary diagram showing the regions where Type I and Type II hot corrosion, as well as alloy induced acidic fluxing hot corrosion, predominate as a function of temperature and SO_3 partial pressure. This diagram also indicates the regions where extensive sulfide formation followed by oxidation of these sulfides is proposed to be a significant form of degradation

important alloying elements. It is probable that all may not agree with what has been presented, but it is hoped that such disagreement will drive research to further clarify these two important forms of deposit-induced degradation at elevated

temperatures. Research topics that are inferred to be important for elaboration of certain aspects of hot corrosion processes are identified in the following:

An important aspect of the Type II degradation mechanism involves the counter diffusion of Co^{3+} and Co^{2+} ions through the liquid sulfate solution. The degradation of other alloys such as NiCrAlY under Type II conditions should be examined since counter diffusion of nickel ions may be less favorable than cobalt. Such studies should also examine the influence of Cr, Al, Ni and Co on Type II attack.

The proposed transition from Type I and Type II attack to a degradation mechanism involving sulfide formation and oxidation of these sulfides should be confirmed at 700 and 900 °C at high SO_3 pressures.

The major amount of experimental data on hot corrosion induced by Na_2SO_4 is at 700 and 900 °C. The attack of CoCrAlY and NiCoCrAlY at 800 °C in an oxygen–SO_2 gas mixture that will produce a liquid sulfate solution should be studied to examine the effect of temperature in more detail.

The effect of Mo on the hot corrosion of alloys at 900 °C is not totally clear. It is well documented that Mo causes alloy-induced acidic fluxing in gas mixtures with low SO_3 partial pressures. However, there are also results that indicate Mo may cause less hot corrosion attack. This may be due to a change in the degradation mechanisms at low and high SO_3 pressures. It is necessary to perform experiments to clarify the effect of Mo on hot corrosion attack at 900 °C.

While not discussed in this paper, the addition of platinum to alloys has been shown to improve cyclic oxidation resistance as well as resistance to Type I and Type II hot corrosion attack [21]. Work to examine the effects of platinum on the hot corrosion of alloys is also recommended.

Acknowledgments G. H. Meier and B. Gleeson are thanked for helpful discussions and assistance in preparing this paper. The Office of Naval Research (ONR) is gratefully acknowledged for support in preparing this paper as well as for many research efforts dealing with hot corrosion attack.

References

1. J. Stringer, *Annual Review of Materials Research* **7**, 477 (1976).
2. Y. S. Zhang and R. A. Rapp, *Journal of Metals* **46**, 47 (1994).
3. F. S. Pettit and C. S. Giggins, in *Superalloys II*, eds. C. T. Sims, N. S. Stoloff, and W. C. Hagel (John Wiley and Sons, New York, NY, 1987).
4. P. Hancock, *Corrosion of Alloys at High Temperatures in Atmospheres Consisting of Fuel Combustion Products and Associated Impurities*, (Her Majesty's Printing Office, London, 1968).
5. K.-Y. Jung, F. S. Pettit, and G. H. Meier, *Materials Science Forum* **595–598**, 805 (2008).
6. N. S. Bornstein and M. A. DeCrescente, *Transactions of the Metallurgical Society of AIME* **245**, 1947 (1969).
7. L. F. Aprigliano, Burner Rig Simulation of Low Temperature Hot Corrosion. David W. Taylor Naval Ship Research and Development Center, Report MAT-77-68, November, 1977.
8. W. T. Reid, *External Corrosion and Deposits in Boilers and Gas Turbines*, (Elsevier, New York, 1971).
9. A. U. Seybolt, *Transactions of the Metallurgical Society of AIME* **242**, 1955 (1968).
10. N. S. Bornstein and M. A. DeCrescente, *Metallurgical Transactions* **2**, 2875 (1971).

11. R. A. Rapp and K. S. Goto, in *Molten Salts*, eds. J. Braunstein and J. R. Selman (The Electrochemical Society, 9, Pennington, NJ, 1981), p. 81.
12. Y. S. Zhang and R. A. Rapp, *Corrosion* **43**, 348 (1987).
13. J. A. Goebel and F. S. Pettit, *Metallurgical Transactions* **1**, 1943 (1970).
14. N. Otsuka and R. A. Rapp, *Journal of the Electrochemical Society* **137**, 46 (1990).
15. A. K. Mishra, *Journal of the Electrochemical Society* **133**, 1038 (1986).
16. K. P. Lillerud and P. Kofstad, *Oxidation of Metals* **21**, 233 (1984).
17. P. Kofstad and G. Akesson, *Oxidation of Metals* **14**, 301 (1980).
18. K. L. Luthra, *Metallurgical Transactions*, **13A**, 1982, 1647 and 1843.
19. R. H. Barkalow and F. S.Pettit, On the oxidation mechanisms for hot corrosion of CoCrAlY coatings in marine gas turbines. *Proceedings of the 14th Conference on Gas Turbine Materials in a Marine Environment* (Naval Sea Systems Command, Annapolis, MD, 1979), p. 493.
20. K. T. Chiang, F. S. Pettit, and G. H. Meier, in *High Temperature Corrosion, NACE-6*, ed. R. A. Rapp (National Association of Corrosion Engineers, Houston, TX, 1983), p. 519.
21. J. Schaeffer, G. M. Kim, G. H. Meier, and F. S. Pettit, in *The Role of Active Elements in the Oxidation Behavior of High Temperature Metals and Alloys*, ed. E. Lang (Elsevier, London, 1989), p. 231.